Neurobiology of Disease

The G59S Mutation in p150^{glued} Causes Dysfunction of Dynactin in Mice

Chen Lai,[1]* Xian Lin,[1,2]* Jayanth Chandran,[1] Hoon Shim,[1] Wan-Jou Yang,[1] and Huaibin Cai[1]

[1]Unit of Transgenesis, Laboratory of Neurogenetics, National Institute on Aging, National Institutes of Health, Bethesda, Maryland 20892, and [2]Department of Anatomy, Zhongshan School of Medicine, Sun Yat-Sen University, Guangzhou 510089, China

The G59S missense mutation at the conserved microtubule-binding domain of p150^{glued}, a major component of dynein/dynactin complex, has been linked to an autosomal dominant form of motor neuron disease (MND). To study how this mutation affects the function of the dynein/dynactin complex and contributes to motor neuron degeneration, we generated p150^{glued} G59S knock-in mice. We found that the G59S mutation destabilizes p150^{glued} and disrupts the function of dynein/dynactin complex, resulting in early embryonic lethality of homozygous knock-in mice. Heterozygous knock-in mice, which developed normally, displayed MND-like phenotypes after 10 months of age, including excessive accumulation of cytoskeletal and synaptic vesicle proteins at neuromuscular junctions, loss of spinal motor neurons, increase of reactive astrogliosis, and shortening of gait compared with wild-type littermates and age-matched p150^{glued} heterozygous knock-out mice. Our findings indicate that the G59S mutation in p150^{glued} abrogates the normal function of p150^{glued} and accelerates motor neuron degeneration.

Key words: **dynactin; dynein; p150^{glued}; motor neuron disease; mouse model; ALS**

Introduction

Motor neurons rely heavily on microtubule-based transport of organelles, vesicles and molecules for their normal function and survival (Holzbaur, 2004). Intracellular cargos are transported either away from (anterograde) or toward (retrograde) the cell body by the kinesin and dynein motor protein complexes (Guzik and Goldstein, 2004). Dynactin, a macromolecular complex, has been proposed to facilitate dynein-mediated retrograde transport of vesicles and organelles along microtubules and provides a link between specific cargos, microtubules and cytoplasmic dynein (Schroer, 2004). The dynactin complex consists of at least 10 distinct components, including p45 (Arp1), p50 (dynamitin), and p150^{glued}. Dynactin p150^{glued}, encoded by the dynactin 1 (*Dctn1*) gene, is the largest subunit of the dynactin complex that binds directly to microtubules and the intermediate chain of dynein through its cytoskeleton-associated glycine-rich protein (CAP-Gly) and coiled-coil domains (Holzbaur and Vallee, 1994; Schroer, 2004). Recently, a single-base pair change in the *Dctn1* gene (C957T) resulting in the substitution of serine for glycine at position 59 of p150^{glued} has been associated with a slowly progressive, autosomal dominant form of lower motor neuron disease without sensory symptoms in a North American family (Puls et al., 2003). This G59S substitution located in the highly conserved CAP-Gly domain of p150^{glued} potentially interferes with protein folding, decreases the binding of the mutant protein to microtubules, and leads to an alteration in dynein/dynactin-mediated transport (Puls et al., 2003; Levy et al., 2006). More missense mutations in *Dctn1* have been identified since and are linked to amyotrophic lateral sclerosis (ALS) and frontotemporal dementia (FTD), although how these mutations affect the structure and function of p150^{glued} is unclear (Munch et al., 2004, 2005).

The evidence for a critical role for p150^{glued} *in vivo* comes from the analysis of mutations in *Drosophila* with the homologous gene, *glued.* The heterozygous *glued* mutation leads to the disruption of axon morphology and fast axonal transport (Reddy et al., 1997; Martin et al., 1999), whereas null mutations are lethal early in development (Harte and Kankel, 1982). Furthermore, the integrity of the dynactin complex is essential for maintaining synapse stability at *Drosophila* neuromuscular junctions (NMJ) (Eaton et al., 2002). Overexpression of dynamitin disassembles the dynactin complex, disrupts axonal retrograde transport and induces accumulation of neurofilaments and synaptophysin at the cell periphery of motor neurons, leading to a late-onset progressive motor neuron disease in transgenic mice (LaMonte et al., 2002). Missense point mutations in cytoplasmic dynein heavy chain also result in motor neuron degeneration in heterozygous mutant mice (Hafezparast et al., 2003).

To study the pathogenic mechanism of the G59S mutation *in vivo*, we generated p150^{glued} G59S knock-in mice and p150^{glued} heterozygous knock-out mice. Whereas heterozygous p150^{glued} knock-out mice appeared normal, heterozygous p150^{glued} G59S knock-in mice developed a late-onset, slowly progressive motor

Received Sept. 14, 2007; revised Nov. 1, 2007; accepted Nov. 2, 2007.

This work was supported by the intramural research program of National Institute on Aging/National Institutes of Health. We thank the Transgenic Mouse Core Facility of the Johns Hopkins University for blastocyte injection, Drs. Philip Wong and Fiona Laird (Johns Hopkins University School of Medicine, Baltimore, MD) for sharing their unpublished data, and the National Institutes of Health Fellows Editorial Board for editing this manuscript.

The authors declare no competing financial interests.

*C.L. and X.L. contributed equally to this work.

Correspondence should be addressed to Huaibin Cai, Unit of Transgenesis, Laboratory of Neurogenetics, National Institute on Aging, National Institutes of Health, Building 35, Room 1A116, MSC 3707, 35 Convent Drive, Bethesda, MD 20892-3707. E-mail: caih@mail.nih.gov.

H. Shim's present address: School of Medicine at Virginia Commonwealth University, Richmond, VA 23298.

DOI:10.1523/JNEUROSCI.4226-07.2007

 0270-6474/07/2713982-09$15.00/0

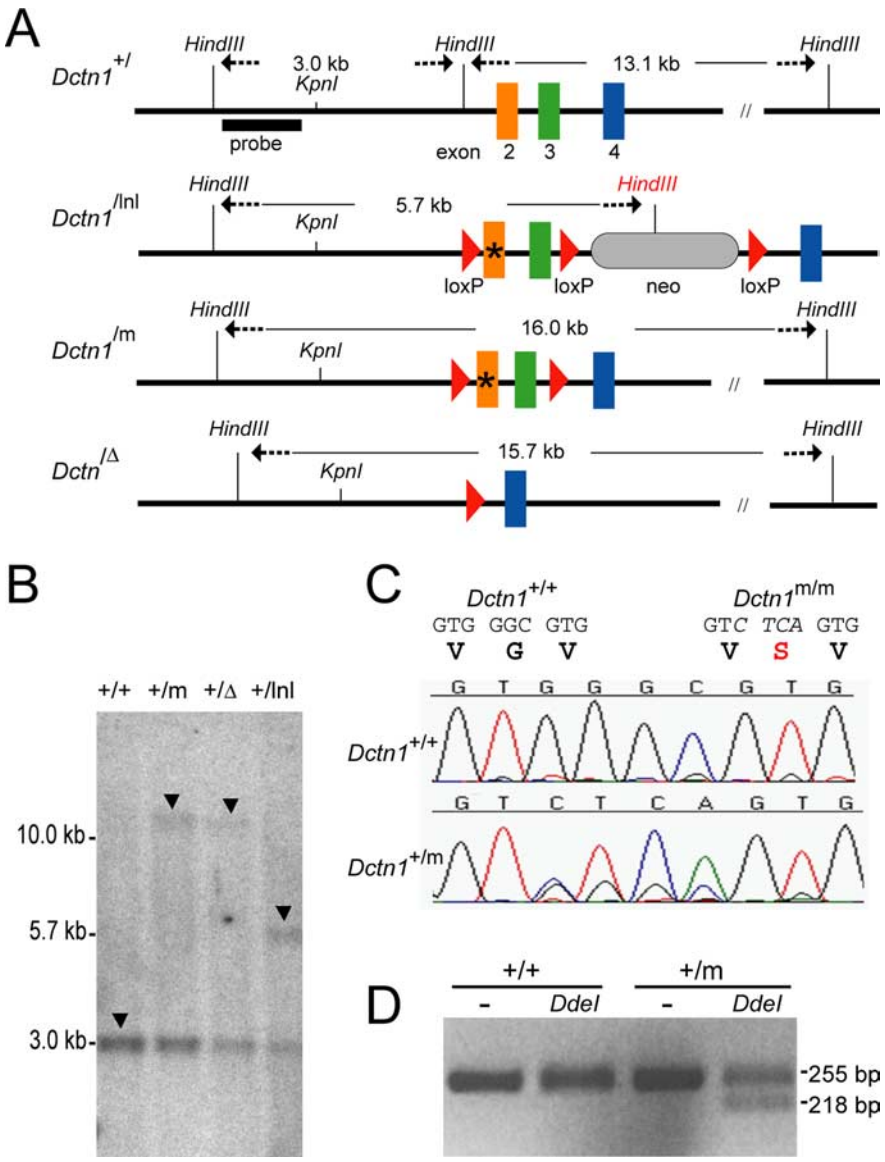

Figure 1. Generation of p150^{glued} G59S knock-in mice. ***A***, A schematic outline of mouse *Dctn1* wild-type (+), floxed neomycin gene (lnl) insertion, G59S knock-in mutant (m), and exons 2 and 3 deletion (Δ) alleles. * represents the mutated region. ***B***, Southern blot analysis of genomic DNA extracted from wild-type and heterozygous mutant mice confirmed the correct targeting of mutated *Dctn1* alleles, which displayed 16.0, 15.7, 5.7, and 3.0 kb *Hin*dIII fragments (arrows) for the lnl, m, Δ, and + alleles, respectively. ***C***, Chromatograms showed the partial sequence of exon2 amplified from RNA extracted from *Dctn1* wild-type (+/+) and heterozygous knock-in (+/m) mice. ***D***, Agarose gel electrophoresis of the RT-PCR products from wild-type (+/+) and *Dctn1*$^{+/m}$ (+/m) after digestion with (+) or without (−) *Dde*I.

neuron disease characterized by abnormal accumulation of neurofilaments and synaptic vesicle proteins at the NMJ, loss of motor neurons, and gait abnormalities. Our findings indicate that the G59S mutation likely exerts a dominant negative effect on the normal function of p150^{glued}, leading to motor neuron degeneration in heterozygous p150^{glued} knock-in mice.

Materials and Methods

Generation of p150^{glued} knock-out and G59S knock-in mice

p150^{glued} protein is encoded by the *Dctn1* gene at mouse chromosome 6. DNA fragments containing *Dctn1* were isolated from a mouse genomic library (Stratagene, La Jolla, CA). A 9.3 kb *Kpn*I/*Sac*II fragment carrying exons 2–8 of *Dctn1* was subcloned into the pBluescript vector for later modifications. To construct the knock-in targeting vector, a 3.1 kb *Hin*dIII/*Spe*I fragment containing exons 2 and 3 of *Dctn1* was modified via introduction of a new *Dde*I site in exon 2 by replacement of nucleotides GGGC with CTCA using QuikChange II XL Site-Directed Mutagenesis Kit (Stratagene, La Jolla, CA), resulting in the substitution of encoded amino acid Glycine with Serine (Fig. 1*A*, *Dctn1*$^{/m}$). To construct the conditional knock-out construct, one copy of a *Loxp* site was inserted into the *Hin*dIII site in front of exon 2 and a 3.4 kb *Xba*I fragment, containing the neomycin-resistance gene flanked with two *Loxp* sites (*lnl*), was inserted into the *Spe*I site immediately after exon 3 (Fig. 1*A*, *Dctn1*$^{/lnl}$). The targeting vector was linearized at a unique *Not*I site and transfected into 129/SvJ ES cells, which were later subjected to G418 selection for 7 d. The G418 resistant ES clones were picked and screened by Southern blot analysis for the correctly targeted clones. Two positive ES clones were expanded and injected into blastocysts. The resulting male chimera mice were bred with wild-type C57BL/6J female mice to obtain *Dctn1*$^{+/lnl}$ mice. *Dctn1*$^{+/lnl}$ mice were then crossed with *Cre* transgenic mice (*EIIa-Cre*) to obtain D*ctn1*$^{+/m}$ and *Dctn1*$^{+/\Delta}$ animals in which both exons 2 and 3 were deleted (Fig. 1*A*). Genomic DNA isolated from mouse livers were digested with *Hin*dIII and subjected to Southern blot analysis using a probe outside of the targeting vector. In addition to a 3.0 kb *Hin*dIII fragment for the wild-type (+) allele, 16.0 kb, 15.7 kb, and 5.7 kb *Hin*dIII fragments were detected for the G59S knock-in mutant (m) allele, the exons 2 and 3 deletion (Δ) allele, and the *loxp* and *neomycin* (lnl) allele, respectively (Fig. 1*B*, arrow). All mutant *Dctn1* mice are a hybrid of 129/SvJ and C57BL/6J strain backgrounds. Once confirmed by Southern blot, mouse genotypes were determined by PCR amplification of tail DNA (*Dctn1*-Ex3F: ACTTCCCCAGAGACTCCTGA and *Dctn1*-Ex4R: CAGTTTGCTGGTCTTTGCAG). The mice were housed in a 12-h light/dark cycle and fed regular diet *ad libitum*. All mouse work follows the guidelines approved by the Institutional Animal Care and Use Committees of the National Institute of Child Health and Human Development.

Transcription analysis of the mutant allele of p150^{glued} G59S knock-in mice

Total RNA purified from the mouse brain by Trizol (Invitrogen) was used as the template for reverse-transcriptase and PCR (RT-PCR) amplification by a pair of *Dctn1* specific primers residing in exon 2 (*Bam*HI-Ex2F: cgcggatccTGTTGGAGCCACACTCTTTG) and 10 (*Eco*RI-Ex10R: ccggaattcTGTAGCGTTCCTTTGCCTCT), respectively. The PCR product was then either digested with *BamH1* and *Eco*RI and subcloned into pBluescript vector for sequence analysis, or used as the template for a second round of PCR amplification using a reverse PCR primer located in exon 4 (Ex4R: CAGTTTGCTGGTCTTTGCAG). The nested PCR product was purified and subjected to *Dde*I digestion. The presence of the G59S allele of *Dctn1*$^{+/m}$ was revealed by the appearance of a smaller DNA band after digestion with *Dde*I (Fig. 1*D*).

Biochemical analysis of the p150^{glued} G59S knock-in mice

Mouse brain or spinal cord was homogenized in TBS buffer (10 mM Tris-HCl pH 7.5, 150 mM NaCl, 5 mM EDTA) plus protease inhibitor cocktails (PI, Roche Bioscience, Palo Alto, CA). Aliquots of homogenates were extracted with 1% Triton X-100 or 2% SDS, respectively, and subjected to immunoblotting. Antibodies used in these studies included

monoclonal anti-p150^{glued} antibody (BD, Transduction Laboratories, Lexington, KY), polyclonal anti-p150^{glued} antibody (Abcam, Cambridge, UK), dynein and p50 antibodies (Chemicon, Temecula, CA), β-tubulin antibody (Covance, Berkeley, CA), and β-actin antibody (Sigma, St Louis, MS).

Sucrose density gradient centrifugation

Brain lysates from wild-type and *Dctn1*$^{+/m}$ mice were homogenized in 20 mM Tris-HCl, pH 7.4, and 1 mM EDTA with PI (Roche). Triton X-100 was added to a final concentration of 0.4%, and the homogenate was clarified by low-speed centrifugation. The resulting supernatant fraction was subjected to 5–20% linear sucrose density gradient centrifugation as described previously (Levy et al., 2006). The gradients were eluted in 1.0 ml fractions, which were resolved by SDS-PAGE and analyzed by Western blot.

Behavior analysis of the p150^{glued} G59S knock-in mice

Rotarod test. Mice were placed onto a rotating rod with auto acceleration from 0 rpm to 40 rpm in 4 min (San Diego Instruments, San Diego, CA). The length of time the mouse stayed on the rotating rod was recorded.

Grip strength measurement. Mice were allowed to use their forepaws or hindpaws to pull or compress a triangular bar attached to a digital force gauge (Ametek, Largo, FL) set up to record the maximal pulling or compressing force. Six measurements were taken for each animal during each test.

Gait analysis. As described previously (Wooley et al., 2005), the TreadScan Gait Analysis System (Clever Sys, Reston, VA) was used to assess the nature of the gait behaviors of the mice. Each mouse was placed into the chamber, onto the treadmill unit. With the speed set at 8 cm/s, each mouse was given 15 s of training time with the treadmill unit. The treadmill was then turned off and the mouse was given 1 min of rest. The treadmill was then turned on again at 8 cm/s and the movement of the mouse was recorded for 20 s at 100 frames per second. The TreadScan software grouped the frames into individual strides for each foot, usually producing between 35 and 50 strides. Stance time, swing time, brake time, propulsion time, stride time, stride length, percentage of stride, and percentage of stance were recorded. Each group of frames was then examined for erroneous data, such as multiple steps recorded as one stride, pauses in the movement resulting in sliding, or the nose and tail being mistaken for a foot. After all erroneous data were removed the rest of the data were exported to Microsoft Excel for calculation of the averages for each parameter of each mouse.

TUNEL assay. Terminal deoxynucleotidyl transferase (TdT) –mediated deoxyuridine triphosphate (dUTP)-rhodamine nick end labeling (TUNEL) assay (Roche) was used to visualize cells undergoing programmed cell death as suggested by the manufacturer. Negative controls were treated similarly except for not being incubated with TdT enzyme. Slides were illuminated using a laser scanning confocal microscope (Zeiss LSM 510, Thornwood, NY).

Histology and immunohistochemical analysis. Mice were perfused via cardiac infusion with 4% paraformaldehyde in cold PBS. To obtain frozen sections, tissues were removed and submerged in 30% sucrose for 24 h and sectioned at 40 μm thickness with a sliding microtome. For paraffin sections, tissues were embedded in paraffin and sectioned at 8 μm thickness by rotary microtome. Antibodies specific for GFAP and synaptophysin (Sigma), and SMI31 and SMI32 (Sternberger Monoclonal, Lutherville, MD) were used as suggested by the manufacturer followed by counterstaining with hematoxylin and eosin (HE). For immunohistochemical analysis, limb muscles from 10- to 24-month-old mice were dissected, fixed, and stained with a synaptophysin antibody (1:500) and SMI32 (1:3000), followed by Alexa Fluor 488-conjugated secondary antibody and Alexa Fluor 568-conjugated α-bungarotoxin (BTX). Z-serial images were collected with confocal microscope (Zeiss). The images presented represent single-projected images derived from overlaying each set of Z-images.

Motor neuron count

The L1 to L5 of lumbar spinal cord was sectioned at 40 μm thickness. Every 12 coronal sections was selected and stained with 0.1% Cresyl Violet (Nissl staining). The criteria for a motor neuron included a round, open, pale nucleus (not condensed and darkly stained), globular Nissl staining of the cytoplasm, and a diameter of ~30–45 μm. More than 25 sections were counted for each animal.

Statistical analysis

Statistical analysis was performed using the StatView program (SAS Institute Inc, version 5.0). Data are presented as means ± SEM. Statistical significances were determined by comparing datasets of different groups using ANOVA or Log rank tests. Differences were considered significant with $p < 0.05$.

Results

Generation of p150^{glued} G59S knock-in mice

To study the role of the p150^{glued} G59S mutation in the development of motor neuron disease, we generated a series of *Dctn1* mutant mice (Fig. 1*A*). The targeted gene replacement of *Dctn1*$^{+/m}$, *Dctn1*$^{+/\Delta}$, and *Dctn1*$^{+/lnl}$ mice was verified by Southern blot in which 16.0, 15.7, 5.7, and 3.0 kb *Hin*dIII fragments were detected, corresponding to the G59S knock-in (m) allele, exon 2 and 3 deletion (Δ) allele, *loxp* and *neomycin* (lnl) insertion allele, and wild-type allele (+), respectively (Fig. 1*B*, arrow). To examine the expression of *Dctn1*$^{+/m}$ mutant allele, a pair of primers residing at exon 2 and 10 of *Dctn1* was used for RT-PCR of total RNA extracted from *Dctn1*$^{+/m}$ mouse brain. The replacement of *GGGC* with *CTCA* in the exon 2 of the mutant allele was confirmed by direct sequencing of purified RT-PCR product (Fig. 1*C*, bottom). A second reverse primer located at exon 4 in combination with the same forward primer at exon 2 were used to amplify a 255 bp PCR product from both wild-type and *Dctn1*$^{+/m}$ samples, which was then digested with *Dde*I. After *Dde*I digestion, a shorter 218 bp band was only detected in *Dctn1*$^{+/m}$ samples, which further confirmed the expression of *Dctn1* mutant allele (Fig. 1*D*).

To compare the expression levels of both wild-type and mutant *Dctn1* alleles in the *Dctn1*$^{+/m}$ mouse brain, we subcloned the RT-PCR product of *Dctn1* exons 2 through 10 into a plasmid vector and randomly picked 32 clones for sequencing. Among these 32 clones, 18 contained the mutated sequence, indicating an equal expression of both wild-type and mutant *Dctn1* alleles in the *Dctn1*$^{+/m}$ mouse brain. Except for the designed mutations at exon 2, no other sequence variation was found in *Dctn1* mutant clones, suggesting that the genetic modification of *Dctn1* does not alter the transcription of the mutant allele.

Embryonic lethality is observed in homozygous p150^{glued} G59S knock-in mice

Previous studies suggest that the G59S mutation in p150^{glued} compromises its binding affinity to microtubules and likely leads to dysfunction of the dynein/dynactin complex (Puls et al., 2003; Levy et al., 2006). To examine the functional consequence of the G59S mutation in p150^{glued}, we intercrossed heterozygous *Dctn1*$^{+/m}$ mice to obtain homozygous *Dctn1*$^{m/m}$ mice. However, no *Dctn1*$^{m/m}$ offspring were obtained from *Dctn1*$^{+/m}$ crosses. The ratio of wild-type and *Dctn1*$^{+/m}$ mice was 1:2, suggesting that the homozygous *Dctn1*$^{m/m}$ mice are embryonically lethal. We then set up timed pregnant mating of heterozygous *Dctn1*$^{+/m}$ mice and collected embryos at different gestation stages. At 9.5 d post coitus (dpc), the wild-type embryo had 21–29 pairs of somites, a well developed heart and CNS, and condensation of forelimb buds near the 8th–12th somite pairs (Fig. 2*A*). The littermate *Dctn1*$^{m/m}$ embryo, however, had severe gastrulation problems. The development of *Dctn1*$^{m/m}$ embryos was likely arrested at approximately 8.0 dpc in which the neural tube was only partially formed and no typical somite could be identified (Fig.

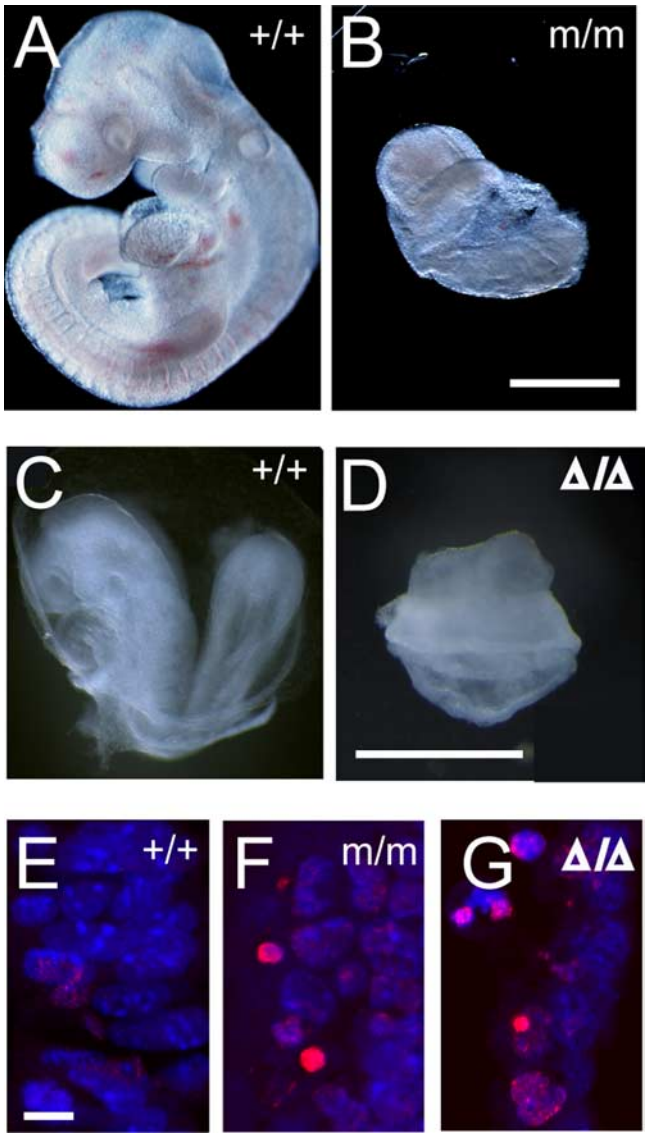

Figure 2. Homozygous *Dctn1* knock-in mice were embryonic lethal. ***A***, ***B***, Wild-type (+/+) and *Dctn1*$^{m/m}$ (m/m) embryos at 9.5 dpc. Scale bar, 500 μm. ***C***, ***D***, Wild-type (+/+) and *Dctn1*$^{\Delta/\Delta}$ (Δ/Δ) were at 8.5 dpc. Scale bar, 600 μm. ***E–G***, TUNEL staining (red) revealed increased programmed cell death in *Dctn1*$^{m/m}$ (m/m; ***F***) and *Dctn1*$^{\Delta/\Delta}$ (Δ/Δ; ***G***) embryos compared with wild-type controls (+/+; ***E***). Nuclei were stained with ToPro-3 (blue). Scale bar, 10 μm.

2*B*). The homozygous deletion of *Dctn1* (*Dctn1*$^{\Delta/\Delta}$) also caused early embryonic lethality (Fig. 2*C*,*D*). The development of *Dctn1*$^{\Delta/\Delta}$ embryo was arrested at approximately 7.5 dpc (Fig. 2*D*) compared with the wild-type littermate control at 8.5 dpc (Fig. 2*C*). In contrast, no significant developmental alterations were observed in heterozygous *Dctn1*$^{+/m}$ and *Dctn1*$^{+/\Delta}$ embryos compared with their wild-type littermate controls (data not shown).

Increased numbers of TUNEL positive cells were also observed in *Dctn1*$^{m/m}$ (Fig. 2*F*) and *Dctn1*$^{\Delta/\Delta}$ (Fig. 2*G*) embryos compared with wild-type (Fig. 2*E*) and heterozygous littermates (data not shown), indicating an augmentation of apoptotic cell death in *Dctn1*-deficient embryos. The early embryonic lethality of *Dctn1*$^{m/m}$ and *Dctn1*$^{\Delta/\Delta}$ mice is consistent with the essential function of the dynein/dynactin complex in cell proliferation and suggests that the G59S mutation in p150^{glued} severely disrupts the normal function of dynactin.

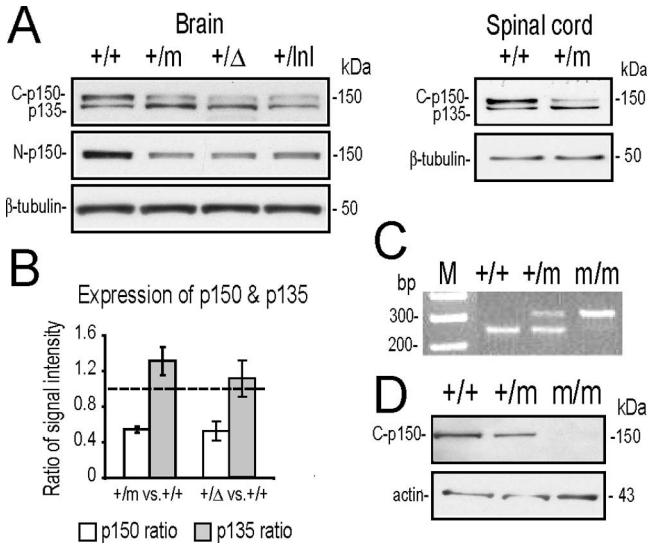

Figure 3. The G59S mutation destabilized p150^{glued} protein. ***A***, Western blot analyses revealed the expression of p150^{glued}/p135 (top; detected by the p150^{glued} C-terminal antibody, C-p150) and p150^{glued} alone (middle; detected by p150^{glued} N-terminal antibody, N-p150) in brains and spinal cords of wild-type (+/+), *Dctn1*$^{+/m}$ (+/m), *Dctn1*$^{+/\Delta}$ (+/Δ), and *Dctn1*$^{+/Inl}$ (+/Inl) mice. The expression of β-tubulin (bottom) was used as a loading control. ***B***, Bar graph shows reduced accumulation of p150^{glued} in *Dctn1*$^{+/m}$ and *Dctn1*$^{+/\Delta}$ brains compared with wild-type controls, whereas the expression of alternative spliced p135 was slightly increased in these animals. Data are means ± SEM. ***C***, Genotyping of wild-type (+/+), *Dctn1*$^{+/m}$ (+/m), and *Dctn1*$^{m/m}$ (m/m) embryos by PCR amplification of genomic DNA prepared from yolk sacs. ***D***, Western blot analyses using p150^{glued} C-terminal antibody revealed the absence of p150^{glued} protein from *Dctn1*$^{m/m}$ (m/m) embryos (top). The expression of β-actin (bottom) was used as a loading control.

The G59S mutation destabilizes p150^{glued} protein

Crystal structures of the CAP-Gly domain in the p150^{glued} protein indicate that the Gly-59 residue is required for maintaining the folding of the three-layer β-sheet structure (Li et al., 2002). It may explain why over-expression of the p150^{glued} G59S mutant protein induces the formation of aggregates in heterologous cell lines (Levy et al., 2006). We examined the expression of p150^{glued} protein in *Dctn1*$^{+/+}$, *Dctn1*$^{+/m}$, *Dctn1*$^{+/\Delta}$, and *Dctn1*$^{+/Inl}$ mouse brains using antibodies that specifically recognize the C-terminal (Fig. 3*A*, top) or N-terminal (Fig. 3*A*, middle) of p150^{glued}. The p150^{glued} C-terminal antibody (C-p150) recognized a doublet of 150 and 135 kDa bands in mouse brain as previously described (Tokito et al., 1996). The 135 kDa band is encoded by an alternative splicing variant of *Dctn1* gene that lacks the first 5 coding exons (Tokito et al., 1996). The p150^{glued} N-terminal antibody (N-p150) raised against the microtubule binding domain of p150^{glued}, reacts only with wild-type full-length p150^{glued} but not with the p150^{glued} G59S mutation or N-terminal truncated p135 variant (Levy et al., 2006). We found that the level of p150^{glued} was reduced by 50% in adult *Dctn1*$^{+/m}$, *Dctn1*$^{+/\Delta}$, and *Dctn1*$^{+/Inl}$ mouse brains and spinal cords (Fig. 3*A*,*B*). Moreover, p150^{glued} protein was not detectable in *Dctn1*$^{m/m}$ mouse embryos collected from 7 to 9 dpc (Fig. 3*C*,*D*). These results suggest that p150^{glued} G59S mutant protein is either quickly degraded or forms detergent insoluble aggregates.

The *Dctn1* p135 isoform is particularly enriched in neural tissues (Tokito et al., 1996), which may explain why it is undetectable in 8.0 dpc mouse embryos (Fig. 3*D*). The level of p135 was comparable among wild-type, *Dctn1*$^{+/m}$ and *Dctn1*$^{+/\Delta}$ mouse brains (Fig. 3*A*,*B*). Although the exact function of p135 remains elusive, it may regulate the function of dynactin complex

by competing with p150^{glued} for binding with dynein and other dynactin subunits (Melloni et al., 1995).

Dynein/dynactin complex remains intact in *Dctn1*$^{+/m}$ mice

The vertebrate dynactin complex has been reported to migrate as a ~19S protein heteromultimer resolved by 5–20% sucrose gradient sedimentation (Levy et al., 2006). To test the integrity of the dynactin complex in *Dctn1*$^{+/m}$ mice, we performed sedimentation analysis on a 5–20% sucrose gradient using brain (Fig. 4*A*,*B*) and spinal cord (data not shown) extracts from wild-type and *Dctn1*$^{+/m}$ mice. The distribution of the dynactin complex, including p150^{glued}, p135, and p50, covered a relatively broader region from fraction 4–7 compared with that of dynein complex, but all proteins in the complex peaked near the 19S fraction (fraction 6) (Fig. 4*A*,*B*). We found that the migration patterns of p150^{glued}, p135, p50, and dynein intermediate chain from *Dctn1*$^{+/m}$ brains were very similar to those from wild-type controls (Fig. 4*A*,*B*), indicating that the G59S mutation in p150^{glued} causes no obvious alteration in the composition of the dynactin and dynein complexes in *Dctn1*$^{+/m}$ mice.

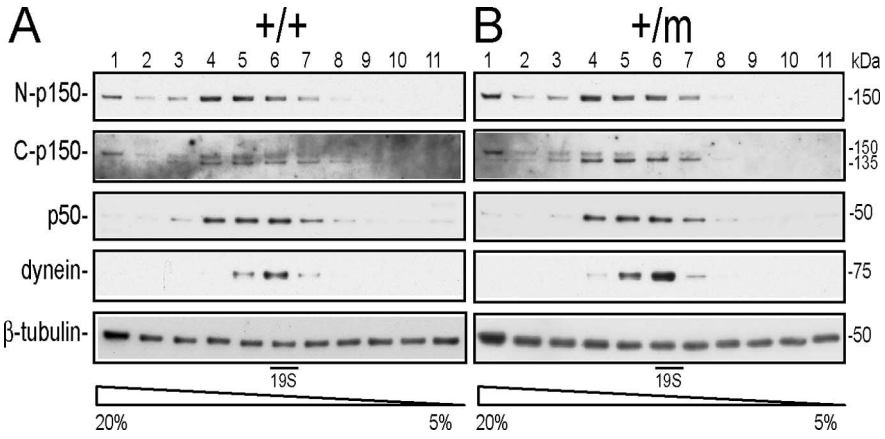

Figure 4. Dynein/dynactin complex remains intact in *Dctn1*$^{+/m}$ mice. Density gradient centrifugation showed that p150^{glued} and its alternative splicing variant, p135, predominantly migrated at ~19S in a 5–20% sucrose gradient similar to dynein and p50 in wild-type (+/+) (***A***) and *Dctn1*$^{+/m}$ (+/m) (***B***) samples prepared from brains. The expression of β-tubulin was used here as a loading control.

Accumulation of neurofilament and synaptophysin at neuromuscular junctions of *Dctn1*$^{+/m}$ mice

Retrograde transport of neurofilaments (NF) along axons has been observed *in vivo* and *in vitro* cell culture models (Glass and Griffin, 1991; Watson et al., 1993). The dynein/dynactin complex associates with NF and is responsible for retrograde transport of NF (Shah et al., 2000). Knock-down of dynein with siRNA *in vitro* significantly diminishes the occurrence of retrograde NF movement without affecting anterograde NF movement, resulting in an accumulation of NF at the axon terminals (He et al., 2005). Because of the significant reduction of p150^{glued} in *Dctn1*$^{+/m}$ and *Dctn1*$^{+/\Delta}$ mice, we examined whether the retrograde transport of NF was affected in motor neurons of these mice. The endplates of neuromuscular junctions (NMJ) of gastrocnemius muscle, in which axons of spinal motor neurons terminate, were visualized by α-bungarotoxin (BTX) staining that specifically labels acetylcholine receptors (AChRs) at the postsynaptic sites. SMI32, a mouse monoclonal antibody reacting with a nonphosphorylated epitope in neurofilament H (NF-H), was used to detect the expression of NF at axon terminals. SMI32 immunoreactivity was restricted to thick axons that terminated at entry points of NMJ of wild-type mice at 10 months of age (Fig. 5*A*, top), whereas a significant accumulation of SMI32 immunoreactivity was observed at the NMJ of littermate *Dctn1*$^{+/m}$ mice that overlapped with BTX staining (Fig. 5*A*, middle). The abnormal accumulation of NF at NMJ of *Dctn1*$^{+/m}$ mice indicates that the G59S mutation in p150^{glued} further compromises the normal function of dynactin, because the loss of one allele of *Dctn1* gene in 13-month-old *Dctn1*$^{+/\Delta}$ mice did not cause a similar accumulation of NF (Fig. 5*A*, bottom).

In addition to NF, synaptophysin, an integral membrane protein associated with small synaptic vesicles is also retrogradely transported by the dynein and dynactin complex (Li et al., 2000). Similar to NF, a significant accumulation of synaptophysin immunoreactivity was observed at the NMJ of *Dctn1*$^{+/m}$ mice compared with wild-type littermate controls (Fig. 5*B*, top and middle) and 13-month-old *Dctn1*$^{+/\Delta}$ mice (Fig. 5*B*, bottom).

Motor neuron degeneration of *Dctn1*$^{+/m}$ mice

To investigate whether the G59S mutation in p150^{glued} leads to motor neuron degeneration, we counted the numbers of motor neurons in lumbar spinal cords from 5 pairs of 4 and 16-month-old *Dctn1*$^{+/m}$ mice and their wild-type littermates (Fig. 6*A–E*). The criteria for a motor neuron included a round, open, pale nucleus (not condensed and darkly stained), globular Nissl staining of the cytoplasm, and a diameter of ~30–45 μm (Fig. 6*C*,*D*). More than 25 coronal sections evenly sampled from L1 to L5 of the lumbar spinal cord were counted for each animal. There was no significant difference in numbers of spinal motor neurons between 4-month-old *Dctn1*$^{+/m}$ mice and their wild-type littermates (+/+: 15.18 ± 0.31, $n = 147$ vs +/m: 15.87 ± 0.26, $n = 150$, $p = 0.09$). However, as shown in Figure 6*E*, the number of motor neurons per section in *Dctn1*$^{+/m}$ mice was reduced significantly (12.98 ± 0.22, $n = 141$, $p < 0.001$) compared with wild-type littermate controls (15.10 ± 0.57, $n = 149$). The number of motor neurons in age-matched *Dctn1*$^{+/\Delta}$ mice ($n = 3$) was also slightly decreased but not statistically significant compared with wild-type controls (14.26 ± 0.68, $n = 90$, $p = 0.7$).

To examine whether mutant p150^{glued} forms intracellular aggregation, we stained the spinal motor neurons of *Dctn1*$^{+/m}$ mice with an antibody against the C-terminal of p150^{glued} (Fig. 6*G*). The staining pattern of p150^{glued} in spinal motor neurons was very similar between wild-type (Fig. 6*F*) and p150^{glued} G59S mutant mice. No obvious aggregation of p150^{glued} was detected within the soma of spinal motor neurons in p150^{glued} G59S mutant mice (Fig. 6*G*). To identify any other neuropathological abnormalities associated with motor neuron degeneration, we examined spinal cord sections of 16-month old *Dctn1*$^{+/m}$ mice with a series of neuropathological markers. More glial fibrillary acidic protein (GFAP)-positive cells were observed in the spinal cord of *Dctn1*$^{+/m}$ mice compared with wild-type controls (Fig. 6*H*,*I*). But, no significant alteration in ubiquitin or phosphorylated neurofilament staining was found in *Dctn1*$^{+/m}$ motor neurons (data not shown).

Motor behavior defects of *Dctn1*$^{+/m}$ mice

To evaluate whether the observed motor neuron degeneration leads to movement disorders in *Dctn1*$^{+/m}$ mice, a cohort of 21

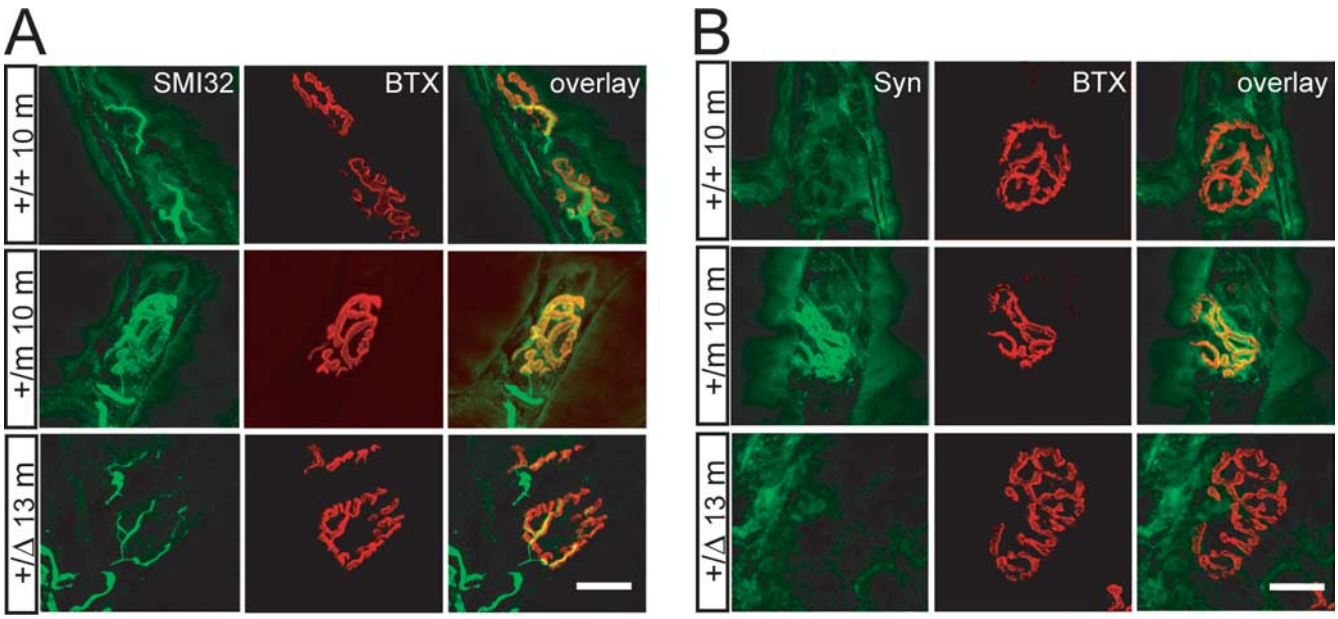

Figure 5. Accumulation of neurofilament and synaptophysin at the NMJ of *Dctn1*$^{+/m}$ mice. ***A***, Motor neurons axons revealed by SMI32 staining terminated at endplates visualized by BTX staining. Increased accumulation of NF was observed at NMJ of gastrocnemius muscle sections from *Dctn1*$^{+/m}$ (+/m 10m) mice at 10 months of age compared with wild-type (+/+ 10 m) littermate controls and *Dctn1*$^{+/\Delta}$ (+/Δ 13 m) mice at 13 months of age. ***B***, Similar to NF, elevated accumulation of synaptophysin (Syn) was observed at NMJ of gastrocnemius muscle sections from *Dctn1*$^{+/m}$ (+/m 10 m) mice at 10 months of age compared with wild-type (+/+ 10 m) littermate controls and *Dcrn1*$^{+/\Delta}$ (+/Δ 13 m) mice at 13 months of age. Muscle section thickness, 10 μm. Scale bars, 20 μm.

male mice (9 for wild-type and 12 for *Dctn1*$^{+/m}$) was examined with a battery of motor behavioral tests. Wild-type and *Dctn1*$^{+/m}$ mice showed no significant differences in performance in either the accelerating rotarod or grip strength at 10 and 16 months of age (data not shown). Because older patients carrying the G59S mutation in p150^{glued} had steppage gait (Puls et al., 2005), and *SOD1*^{G93A} mice, a well established mouse model for ALS, developed significantly shorter stride length (Gurney et al., 1994; Puttaparthi et al., 2002; Puls et al., 2005), we examined the gait of *Dctn1*$^{+/m}$ mice using the Treadscan Gait Analysis system. We quantified the stride length of wild-type and *Dctn1*$^{+/m}$ mice at 4 and 16 months of age. The stride length of *Dctn1*$^{+/m}$ mice at 4 months of age was comparable between wild-type and mutant mice (+/+: 58.39 ± 0.71 mm vs +/m: 57.33 ± 1.01 mm, $n = 5$ each, $p = 0.39$), but it was significantly shorter at 16 months of age (47.98 ± 0.85 mm, $n = 12$, $p = 0.03$) compared with that of wild-type controls (50.75 ± 0.86 mm, $n = 9$).

The G59S Mutation in *Dctn1* does not affect the progression of motor neuron degeneration in SOD1^{G93A} transgenic mice

Similar to the G59S mutation in p150^{glued}, two missense mutations in cytoplasmic dynein heavy chain also result in progressive motor neuron degeneration in heterozygous mutant mice (Hafezparast et al., 2003). Interestingly, these dynein mutations prolong the survival of SOD1^{G93A} transgenic mice (Kieran et al., 2005; Teuchert et al., 2006), raising the question as to whether the G59S mutation in p150^{glued} causes a similar effect. To address this question, we cross-bred SOD1^{G93A} mice, the same strain of mice used in Kieran's and Teuchert's studies (Kieran et al., 2005; Teuchert et al., 2006), with *Dctn1*$^{+/m}$ mice and examined the onset of paralysis of SOD1^{G93A} and *Dctn1*$^{+/m}$ double transgenic mice. We found that the onset of paralysis was comparable between SOD1^{G93A} single transgenic mice with SOD1^{G93A} and *Dctn1*$^{+/m}$ double mutant mice (log rank test, $p = 0.49$) (Fig. 7), suggesting that deficiency in *Dctn1* gene does not significantly affect the pathogenesis of SOD1^{G93A} transgenic mice.

Discussion

The growth and maintenance of the axon, as well as the movement of cargo between the cell body and the distal tip of the axon, rely on the mechanism of axonal transport (Guzik and Goldstein, 2004). The dynein/dynactin complex plays an essential role in retrograde axonal transport (Allan, 1996; Karki and Holzbaur, 1999; Schroer, 2004). Mutations in cytoplasmic dynein heavy chain and over-expression of dynactin p50 subunit have been shown to affect axonal transport and induce progressive motor neuron degeneration (LaMonte et al., 2002; Hafezparast et al., 2003). The present study demonstrates for the first time that a mouse model carrying a MND-linked G59S substitution in the dynactin p150^{glued} subunit develops many symptoms related to ALS and MND, such as motor neuron degeneration, reactive astrogliosis, and abnormal gait. Because *Dctn1*$^{+/m}$ mice contain one copy of wild-type allele and one copy of G59S mutant allele, it faithfully replicates the genetic mutation in humans and may serve as a useful animal model for studying the pathogenic mechanism of MND and testing potential therapeutics.

We provided evidence to further demonstrate that p150^{glued} is required for the cellular functions of cytoplasmic dynein (King and Schroer, 2000). *Dctn1*$^{m/m}$ and *Dctn1*$^{\Delta/\Delta}$ mice died before 8.5 dpc, similar to cytoplasmic dynein heavy chain knock-out mice (Harada et al., 1998). The G59S mutation in p150^{glued} does not affect the integrity of the dynein/dynactin complex, except for inducing self-aggregation when over-expressed in cell lines (Levy et al., 2006). In sucrose density gradient centrifugation assays, we did not observe any abnormal distribution of dynein, p50, and p150^{glued} extracted from brain or spinal cord of *Dctn1*$^{+/m}$ mice, nor could we detect any aggregated forms of p150^{glued} from *Dctn1*$^{+/m}$ mouse brains. In fact, we observed an ~50% reduction

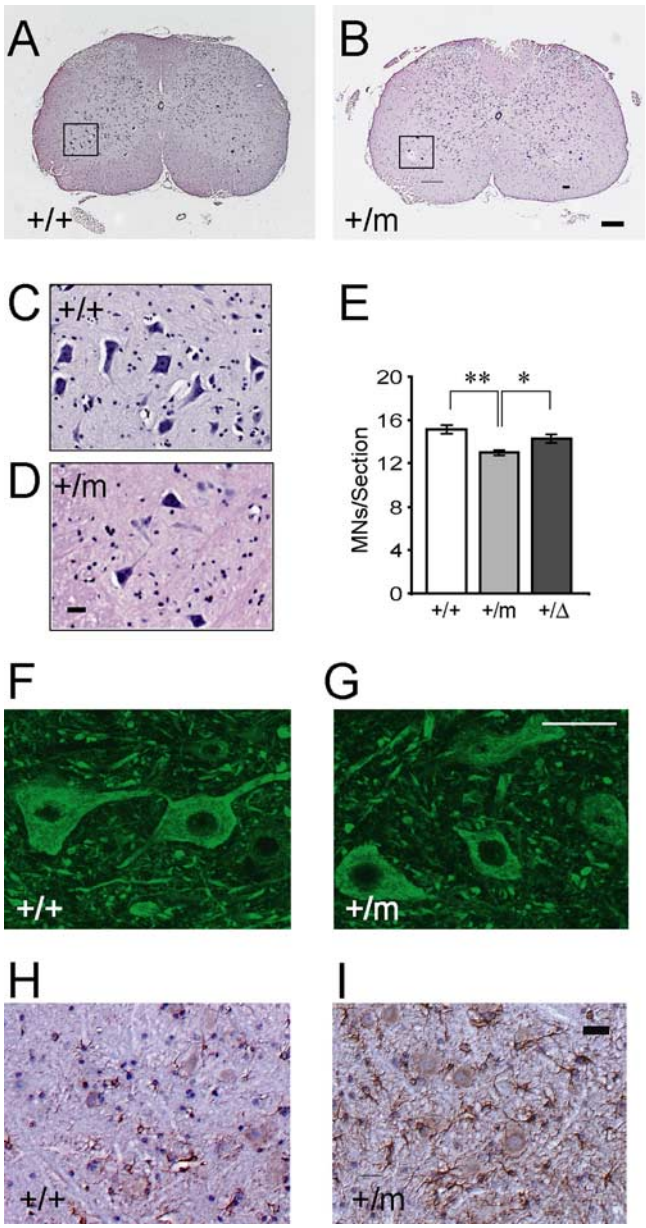

Figure 6. Motor neuron degeneration in *Dctn1*$^{+/m}$ mice (***A–D***) HE staining of coronal sections of lumbar spinal cords revealed motor neurons in wild-type (***A***, ***C***) and *Dctn1*$^{+/m}$ (***B***, ***D***) mice at 16 months of age. The insets (***C***, ***D***) showed motor neurons under higher magnification of the boxed area (***A***, ***B***). Scale bars: main, 100 μm; insets, 50 μm. ***E***, Box graph of numbers of motor neurons per lumbar spinal cord section of wild-type (+/+), *Dctn1*$^{+/m}$ (+/m), and *Dctn1*$^{+/\Delta}$ (+/Δ) mice. *$p < 0.01$ and **$p < 0.001$, respectively. ***F***, ***G***, Representative images of p150^{glued} staining with the antibody against the C-terminal of p150^{glued} in the wild-type (+/+) and *Dctn1*$^{+/m}$ (+/m) lumbar spinal cords. Scale bar, 50 μm. ***H***, ***I***, Representative images of GFAP staining in the wild-type (+/+) and *Dctn1*$^{+/m}$ (+/m) lumbar spinal cords. All the sections were counterstained with HE. Scale bar, 20 μm.

of p150^{glued} in *Dctn1*$^{+/m}$ mouse brains and failed to detect any p150^{glued} from *Dctn1*$^{m/m}$ mouse embryos, suggesting that the G59S mutation in p150^{glued} leads to a rapid degradation of mutant p150^{glued}. Protein structure analysis indicates that the Gly59 and the adjacent Phe88 residues play an important role in the folding of CAP-Gly domain (Li et al., 2002). The substitution of Gly59 with the polar Ser59 residue may hinder its interaction with the side chain of Phe88 and lead to protein misfolding and degradation (Puls et al., 2003). It is not unusual that missense mutations and short in-frame deletions or insertions cause protein misfolding and eventually degradation in genetic diseases (Bross et al., 1999). Misfolded proteins may aggregate if the cellular degradation pathways are compromised, which may explain why p150^{glued} G59S mutant protein aggregates when overexpressed in heterologous cell lines (Levy et al., 2006). We could not detect any p150^{glued} aggregates in the brain or spinal cord of *Dctn1*$^{+/m}$ mice, indicating that the mutant protein is primarily targeted to the degradation pathway *in vivo*. However, we cannot completely rule out the presence of the p150^{glued} G59S mutant protein or its aggregates inside cells.

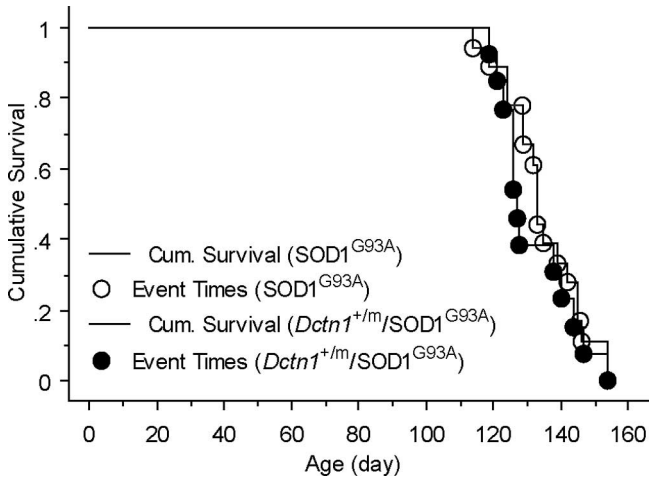

Figure 7. The G59S mutation in p150^{glued} does not affect the survival of SOD1^{G93A} transgenic mice. Kaplan–Meier plot of cumulative probability of survival of SOD1^{G93A}/*Dctn1*$^{+/+}$ ($n = 10$) and SOD1^{G93A}/*Dctn1*$^{+/m}$ mice ($n = 15$).

It is still unclear how the G59S mutation in p150^{glued} affects the activity of dynein. A recent study suggests that the CAP-Gly domain of p150^{glued} enables stable binding of dynein at the plus end of microtubules; whereas the basic domain of p150^{glued} facilitates dynein processivity along a microtubule (Culver-Hanlon et al., 2006). The G59S mutation seems to weaken the binding of p150^{glued} with microtubules (Levy et al., 2006), which may alter the movement of dynein along a microtubule. The speed of retrograde transport in *Dctn1*$^{+/m}$ motor neurons remains to be determined. The increased accumulation of NF and synaptophysin at the tips of motor neuron axons of *Dctn1*$^{+/m}$ mice may result from either a reduction of the speed in retrograde transport or a partial loss of the capacity of dynein/dynactin-mediated retrograde transport, as shown previously in dynein knock-down neurons (He et al., 2005).

The most distinct clinical phenotype of patients carrying the G59S mutation in p150^{glued} is early bilateral vocal fold paralysis that affects the abductor and abductor laryngeal muscles (Puls et al., 2005). Muscle weakness and atrophy in the face, hands, and distal legs were observed later, reflecting motor neuron degeneration in the ventral horn of the spinal cord and hypoglossal nucleus of the medulla. P50 and dynein aggregates were also observed in a subset of motor neurons from an autopsy study on one patient. Consistent with these clinical observations, we detected a significant loss of motor neurons and increased astrogliosis at the lumbar spinal cord of *Dctn1*$^{+/m}$ mice. Because age-matched *Dctn1*$^{+/\Delta}$ mice did not develop any of these neuropathological abnormalities as observed in *Dctn1*$^{+/m}$ mice, our data indicate that a 50% reduction of p150^{glued} alone is not sufficient to cause motor neuron degeneration at the age having been examined. Neither does the increase of p135 account for the motor behavioral and neuropathological deficits observed in

Dctn1$^{+/m}$ mice, because a comparable increase of p135 was also found in *Dctn1*$^{+/\Delta}$ mice. The G59S mutation may exert additional stress to motor neurons through further disruption of the function of dynein/dynactin complex. Alternatively, these results may be also consistent with a toxic-gain-of-function mechanism because the NMJ phenotypes and motor neuron loss were worse in the heterozygous knock-in mice than in the knock-out animals. However, because very little or no p150^{glued} G59S protein was detected in the mutant mouse it is hard to argue the mutant protein may cause any significant effect in cells. Nonetheless, to clearly address this issue, p150^{glued} G59S transgenic mice (developed by Dr. Philip Wong at the Johns Hopkins University) will breed into p150^{glued} heterozygous knock-out background. If the G59S mutation is a dominant-negative mutation, an acceleration of disease progression will be expected from these mice because of a loss of 50% endogenous wild-type protein.

Axonal transport deficits have also been reported in SOD1^{G93A} transgenic mice (Warita et al., 1999), which could be rescued by mutations in dynein, resulting in longer survival of SOD1^{G93A} transgenic mice (Kieran et al., 2005; Teuchert et al., 2006). The detailed molecular interaction between these two mutant proteins is unclear. There is evidence that the aggregates of mutant SOD1 interact with cytoplasmic dynein and alter its subcellular localization in motor neurons (Ligon et al., 2005), which may inhibit dynein activity and lead to motor neuron degeneration. Whether mutations in dynein affect its interaction with SOD1^{G93A} remains unknown. Alternatively, slower retrograde axonal transport as observed in dynein mutant neurons (Kieran et al., 2005) may neutralize the impairment of fast anterograde axonal transport in motor neurons of SOD1^{G93A} transgenic mice and prolong the survival of these mutant mice. Because the G59S mutation in p150^{glued}, which caused a loss of at least 50% of dynein/dynactin activity, did not affect the onset of paralysis or death of SOD1^{G93A} transgenic mice, our data indicate that partial loss of dynein/dynactin-mediated retrograde axonal transport is not sufficient to delay the motor neuron degeneration of SOD1^{G93A} mice. The mechanism by which the p150^{glued} G59S mutation exerts a pathogenic effect is likely different from that of dynein mutations. Alternatively, one can argue that the effects of heterozygous p150^{glued} G59S mutation might be too subtle to affect the severe and rapid disease progression in SOD1^{G93A} mice.

In summary, our study indicates that the G59S mutation in p150^{glued} may play a dominant negative role in the normal function of dynactin, which leads to motor neuron degeneration in the heterozygous mutant mice. The 150^{glued} G59S knock-in mice may serve as a useful tool for studying the pathogenic mechanisms of ALS and MND.

References

Allan V (1996) Motor proteins: a dynamic duo. Curr Biol 6:630–633.

Bross P, Corydon TJ, Andresen BS, Jorgensen MM, Bolund L, Gregersen N (1999) Protein misfolding and degradation in genetic diseases. Hum Mutat 14:186–198.

Culver-Hanlon TL, Lex SA, Stephens AD, Quintyne NJ, King SJ (2006) A microtubule-binding domain in dynactin increases dynein processivity by skating along microtubules. Nat Cell Biol 8:264–270.

Eaton BA, Fetter RD, Davis GW (2002) Dynactin is necessary for synapse stabilization. Neuron 34:729–741.

Glass JD, Griffin JW (1991) Neurofilament redistribution in transected nerves: evidence for bidirectional transport of neurofilaments. J Neurosci 11:3146–3154.

Gurney ME, Pu H, Chiu AY, Dal Canto MC, Polchow CY, Alexander DD, Caliendo J, Hentati A, Kwon YW, Deng HX (1994) Motor neuron degeneration in mice that express a human Cu,Zn superoxide dismutase mutation. Science 264:1772–1775.

Guzik BW, Goldstein LS (2004) Microtubule-dependent transport in neurons: steps towards an understanding of regulation, function and dysfunction. Curr Opin Cell Biol 16:443–450.

Hafezparast M, Klocke R, Ruhrberg C, Marquardt A, Ahmad-Annuar A, Bowen S, Lalli G, Witherden AS, Hummerich H, Nicholson S, Morgan PJ, Oozageer R, Priestley JV, Averill S, King VR, Ball S, Peters J, Toda T, Yamamoto A, Hiraoka Y, et al. (2003) Mutations in dynein link motor neuron degeneration to defects in retrograde transport. Science 300:808–812.

Harada A, Takei Y, Kanai Y, Tanaka Y, Nonaka S, Hirokawa N (1998) Golgi vesiculation and lysosome dispersion in cells lacking cytoplasmic dynein. J Cell Biol 141:51–59.

Harte PJ, Kankel DR (1982) Genetic analysis of mutations at the Glued locus and interacting loci in *Drosophila melanogaster*. Genetics 101:477–501.

He Y, Francis F, Myers KA, Yu W, Black MM, Baas PW (2005) Role of cytoplasmic dynein in the axonal transport of microtubules and neurofilaments. J Cell Biol 168:697–703.

Holzbaur EL (2004) Motor neurons rely on motor proteins. Trends Cell Biol 14:233–240.

Holzbaur EL, Vallee RB (1994) DYNEINS: molecular structure and cellular function. Annu Rev Cell Biol 10:339–372.

Karki S, Holzbaur EL (1999) Cytoplasmic dynein and dynactin in cell division and intracellular transport. Curr Opin Cell Biol 11:45–53.

Kieran D, Hafezparast M, Bohnert S, Dick JR, Martin J, Schiavo G, Fisher EM, Greensmith L (2005) A mutation in dynein rescues axonal transport defects and extends the life span of ALS mice. J Cell Biol 169:561–567.

King SJ, Schroer TA (2000) Dynactin increases the processivity of the cytoplasmic dynein motor. Nat Cell Biol 2:20–24.

LaMonte BH, Wallace KE, Holloway BA, Shelly SS, Ascano J, Tokito M, Van Winkle T, Howland DS, Holzbaur EL (2002) Disruption of dynein/dynactin inhibits axonal transport in motor neurons causing late-onset progressive degeneration. Neuron 34:715–727.

Levy JR, Sumner CJ, Caviston JP, Tokito MK, Ranganathan S, Ligon LA, Wallace KE, LaMonte BH, Harmison GG, Puls I, Fischbeck KH, Holzbaur EL (2006) A motor neuron disease-associated mutation in p150Glued perturbs dynactin function and induces protein aggregation. J Cell Biol 172:733–745.

Li JY, Pfister KK, Brady ST, Dahlstrom A (2000) Cytoplasmic dynein conversion at a crush injury in rat peripheral axons. J Neurosci Res 61:151–161.

Li S, Finley J, Liu ZJ, Qiu SH, Chen H, Luan CH, Carson M, Tsao J, Johnson D, Lin G, Zhao J, Thomas W, Nagy LA, Sha B, DeLucas LJ, Wang BC, Luo M (2002) Crystal structure of the cytoskeleton-associated protein glycine-rich (CAP-Gly) domain. J Biol Chem 277:48596–48601.

Ligon LA, LaMonte BH, Wallace KE, Weber N, Kalb RG, Holzbaur EL (2005) Mutant superoxide dismutase disrupts cytoplasmic dynein in motor neurons. NeuroReport 16:533–536.

Martin M, Iyadurai SJ, Gassman A, Gindhart Jr JG, Hays TS, Saxton WM (1999) Cytoplasmic dynein, the dynactin complex, and kinesin are interdependent and essential for fast axonal transport. Mol Biol Cell 10:3717–3728.

Melloni Jr RH, Tokito MK, Holzbaur EL (1995) Expression of the p150Glued component of the dynactin complex in developing and adult rat brain. J Comp Neurol 357:15–24.

Munch C, Sedlmeier R, Meyer T, Homberg V, Sperfeld AD, Kurt A, Prudlo J, Peraus G, Hanemann CO, Stumm G, Ludolph AC (2004) Point mutations of the p150 subunit of dynactin (DCTN1) gene in ALS. Neurology 63:724–726.

Munch C, Rosenbohm A, Sperfeld AD, Uttner I, Reske S, Krause BJ, Sedlmeier R, Meyer T, Hanemann CO, Stumm G, Ludolph AC (2005) Heterozygous R1101K mutation of the DCTN1 gene in a family with ALS and FTD. Ann Neurol 58:777–780.

Puls I, Jonnakuty C, LaMonte BH, Holzbaur EL, Tokito M, Mann E, Floeter MK, Bidus K, Drayna D, Oh SJ, Brown Jr RH, Ludlow CL, Fischbeck KH (2003) Mutant dynactin in motor neuron disease. Nat Genet 33:455–456.

Puls I, Oh SJ, Sumner CJ, Wallace KE, Floeter MK, Mann EA, Kennedy WR, Wendelschafer-Crabb G, Vortmeyer A, Powers R, Finnegan K, Holzbaur EL, Fischbeck KH, Ludlow CL (2005) Distal spinal and bulbar muscular atrophy caused by dynactin mutation. Ann Neurol 57:687–694.

Puttaparthi K, Gitomer WL, Krishnan U, Son M, Rajendran B, Elliott JL (2002) Disease progression in a transgenic model of familial amyotro-

phic lateral sclerosis is dependent on both neuronal and non-neuronal zinc binding proteins. J Neurosci 22:8790–8796.

Reddy S, Jin P, Trimarchi J, Caruccio P, Phillis R, Murphey RK (1997) Mutant molecular motors disrupt neural circuits in *Drosophila*. J Neurobiol 33:711–723.

Schroer TA (2004) Dynactin. Annu Rev Cell Dev Biol 20:759–779.

Shah JV, Flanagan LA, Janmey PA, Leterrier JF (2000) Bidirectional translocation of neurofilaments along microtubules mediated in part by dynein/dynactin. Mol Biol Cell 11:3495–3508.

Teuchert M, Fischer D, Schwalenstoecker B, Habisch HJ, Bockers TM, Ludolph AC (2006) A dynein mutation attenuates motor neuron degeneration in SOD1(G93A) mice. Exp Neurol 198:271–274.

Tokito MK, Howland DS, Lee VM, Holzbaur EL (1996) Functionally distinct isoforms of dynactin are expressed in human neurons. Mol Biol Cell 7:1167–1180.

Warita H, Itoyama Y, Abe K (1999) Selective impairment of fast anterograde axonal transport in the peripheral nerves of asymptomatic transgenic mice with a G93A mutant SOD1 gene. Brain Res 819:120–131.

Watson DF, Glass JD, Griffin JW (1993) Redistribution of cytoskeletal proteins in mammalian axons disconnected from their cell bodies. J Neurosci 13:4354–4360.

Wooley CM, Sher RB, Kale A, Frankel WN, Cox GA, Seburn KL (2005) Gait analysis detects early changes in transgenic SOD1(G93A) mice. Muscle Nerve 32:43–50.